Optical Engineering

OpticalEngineering.SPIEDigitalLibrary.org

Analytical modeling of blazed gratings on two-dimensional pixelated liquid crystal on silicon devices

Andrés Márquez
Francisco J. Martínez-Guardiola
Jorge Francés
Cristian Neipp
Manuel G. Ramírez
Eva M. Calzado
Marta Morales-Vidal
Sergi Gallego
Augusto Beléndez
Inmaculada Pascual

SPIE.

Andrés Márquez, Francisco J. Martínez-Guardiola, Jorge Francés, Cristian Neipp, Manuel G. Ramírez, Eva M. Calzado, Marta Morales-Vidal, Sergi Gallego, Augusto Beléndez, Inmaculada Pascual, "Analytical modeling of blazed gratings on two-dimensional pixelated liquid crystal on silicon devices," *Opt. Eng.* **59**(4), 041208 (2020), doi: 10.1117/1.OE.59.4.041208

Analytical modeling of blazed gratings on two-dimensional pixelated liquid crystal on silicon devices

Andrés Márquez,[a,b,*] Francisco J. Martínez-Guardiola,[a,b] Jorge Francés,[a,b] Cristian Neipp,[a,b] Manuel G. Ramírez,[a,b] Eva M. Calzado,[a,b] Marta Morales-Vidal,[b] Sergi Gallego,[a,b] Augusto Beléndez,[a,b] and Inmaculada Pascual[b,c]

[a]Universidad de Alicante, Departamento de Física, Ingeniería de Sistemas y Teoría de la Señal, Alicante, Spain

[b]Universidad de Alicante, I.U. Física Aplicada a las Ciencias y las Tecnologías, Alicante, Spain

[c]Universidad de Alicante, Departamento de Óptica, Farmacología y Anatomía, Alicante, Spain

Abstract. Phase spatial light modulators and, in particular, parallel-aligned liquid crystal on silicon (PA-LCoS) microdisplays are widely used to display programmable diffractive optical elements (DOEs). These are pixelated elements with inherent different characteristics when compared with DOEs produced with micro-optics fabrication techniques. Specifically, programmable DOEs may be affected by the fill factor, time-flicker, fringing-field and interpixel cross talk effects, and limited and quantized modulation depth of the LCoS device. Among the multilevel DOEs, we focus on the important case of the blazed gratings. We develop the corresponding analytical expressions for the diffracted field where, as novelties of this work, fill factor and flicker are introduced together with phase depth and the number of quantization levels. Different experimental-based normalizations are considered, which may lead to wrong conclusions if the fill factor is not considered in the expressions. We also analyze the differences arising between one- and two-dimensional pixelated devices. When compared with numerical procedures, our approach provides an analytical expression that facilitates the design, prediction, and discussion of experiments. As an application, we prove, for the limiting case of no interpixel cross talk, that multiorder DOEs cannot be more efficient than the equivalent single-order DOE. We also show how the results for DOEs with a unit fill factor can be adapted to DOEs with a fill factor smaller than one with a very efficient procedure. [DOI: 10.1117/1.OE.59.4.041208]

Keywords: liquid crystal on silicon displays; parallel aligned; phase-only modulation; spatial light modulation; flicker; blazed gratings; diffractive optics; multiorder element.

Paper 191408SS received Oct. 11, 2019; accepted for publication Feb. 4, 2020; published online Feb. 17, 2020.

1 Introduction

Spatial light modulators (SLMs)[1] are nowadays a central element in many modern photonics systems. One of the main capabilities they offer is programmability, defined as the possibility of computer control and tunability of the optical element addressed in real-time, thus adding flexibility to the optical architecture of the optical system. In the case of diffractive optics, they enable the display of programmable diffractive optical elements (DOEs), which can be applied to a large variety of tasks, such as beam shaping,[2] point-spread function engineering,[3] holographic optical traps,[4] or interconnects.[5]

Usually, SLMs enabling phase-only modulation are preferable since light loss is a major concern in most of the applications. This is the case of parallel-aligned liquid-crystal on silicon (PA-LCoS) microdisplays, probably the most widespread SLM technology, which offers very

*Address all correspondence to Andrés Márquez E-mail: andres.marquez@ua.es

0091-3286/2020/$28.00

large resolution together with phase-only operation without coupled amplitude modulation.[6–8] They can be assimilated to linear variable retarders, whose linear retardance varies with the applied voltage. Proper evaluation of these devices has shown that they exhibit fluctuations (flicker) in their retardance values,[9–11] which can be minimized by the proper selection of the waveform sequence addressed,[12,13] among other degradation artifacts, such as the fringing-field effect.[14,15] Physical parameters for SLM devices in general, and LCoS microdisplays in particular, are usually not available. Therefore, important efforts have been dedicated to proper modeling and characterization through reverse-engineering approaches[16,17] so that the operation of these devices can be optimized for applications. In this aspect, we analyzed the effect of flicker on blazed gratings.[18] Among multilevel phase elements, blazed gratings are simpler to evaluate, enabling a deeper insight into the parameters affecting the performance of more complex DOEs. In particular, we found that flicker effects become much less noticeable in blazed gratings when compared with the results addressing uniform screens, therefore, degradation effects due to flicker are very much application dependent.[18] Blazed gratings are not only a useful starting point to get a deeper insight onto the parameters affecting the operation of multilevel phase elements. They are also the basic unit in a variety of applications, such as reconfigurable interconnects for intrachip systems,[19] in fiber optics,[20,21] or in free-space laser communications.[22,23] They are also the basic element in beam-steering applications,[24,25] where many developments are directed to one-dimensional (1D) pixelated devices, i.e., linear arrays, usually called liquid crystal optical phased array (LC-OPA)[24,25] when using LCs as the tunable material.

One important point of programmable DOEs is that they are displayed onto a pixelated device, whose modulation range is both limited and quantized. When displaying a phase DOE, its wrapped phase function modulus 2π rad is usually considered,[26] thus, a 2π rad phase depth is required from the SLM. Smaller phase depth and/or small number of phase quantization levels have also an influence on the DOE introducing more background noise and/or diminishing its efficiency.[27] DOEs produced by binary optics[28–30] share most of these characteristics. However, there is something that is specific of programmable DOEs: what we call the pixel aperture ratio or fill factor. This is the ratio of the pixel clear aperture versus its width, usually calculated in areal terms. In SLM devices, the fill factor is smaller than the one due to the interpixel gap necessary to electrically isolate neighboring pixel electrodes, which is used in some SLM technologies for the wiring necessary to access electrical signals to the pixels.[31]

In many LCoS microdisplays, this interpixel gap has no reflective coating and thus absorbs light, as can be seen, for example, in the LCoS backplane images included in the papers by Lingel et al.,[15] Lu et al.[32] and Chian and Wu.[33] Actually, in the latter, they consider a zero reflectance in the interpixel gap for their numerical modeling. Reflectivity and flatness of the backplane has been an important issue along the years in the development of LCoS microdisplays. LCoS backplane fabrication has adapted the CMOS microelectronics technology from silicon fabs, incorporating additional steps necessary to block leakage of incident light to avoid photocurrent generation in the underlying CMOS structure, to enhance the reflectance of the pixel electrodes, and to achieve the stringent degree of flatness necessary for optical applications.[7,34,35] Nowadays, it is possible to fabricate the LCoS backplane with a dielectric mirror on top, thus, the interpixel gap is also reflective.[7,36,37] This is still a subject of ongoing research, as discussed by Yang and Chu,[36] since the addition of the dielectric mirror enhances the existence of fringing-field effects and diminishes the effective voltage drop across the LC layer.

In this paper, we focus on the LCoS microdisplays, whose interpixel gap is absorbent, which are probably the most widespread devices. Fill factors closer to one are desired since this means that less light is absorbed in the pixelated device. In this paper, we will show that it modifies the global efficiency of the SLM and also affects the general expressions for the diffracted field by the programmable phase element. The latter is not usually considered; thus, it may lead to a bad assessment of the results in experiments.

In the literature for blazed gratings, analytical expressions for the diffracted field are not complete since they usually express the case for 2π rad phase depth and for fill factor equal to 1, which is only valid for micro-optics DOEs. The one exception is Gil-Leyva et al.:[19] they included the fill factor but only for the specific case when phase depth is 2π rad. The procedure they followed for the calculation, Fourier Optics approach, does not separate the influence of fill factor, multislit interference, and interaction between periods since both the pixel and the grating

period periodicities cannot be easily decoupled. In this paper, we consider the diffraction integral-based approac[26] and we will show how, even though all parameters are included, we can separate the three different factors influencing the far-field profile to obtain a simple analytical closed form.

In the present paper, for blazed gratings, we develop the corresponding analytical expressions for the diffracted field spatial profile and for the diffraction efficiency at the different orders, whereas one of the novelties in the work, we include all the parameters together with the fill factor and the flicker. In Sec. 2, we show the basic theory for far-field diffraction by blazed gratings, which are the multilevel phase elements used in the study. We consider a linear dependence of flicker amplitude with the phase level since this enables to obtain a useful analytical model. The case for 1D and two-dimensional (2D) pixelated devices is analyzed, and three different experimental-based normalizations are applied and discussed. In Sec. 3, we provide simulated results, showing the usefulness of our approach. Eventually, the main conclusions of the paper are given in Sec. 4.

2 Pixelated Blazed Gratings: Far-Field Analytical Expressions

2.1 *Two-Dimensional Pixelated Devices and Linear Arrays*

In diffractive optics, one of the main parameters to evaluate a DOE is the diffraction efficiency. It is usually expressed as the intensity diffracted into the desired region in the output plane normalized by the total amount of incident light even though other normalizations are also useful. In the case of blazed gratings, the desired output region is typically the first diffraction order, which corresponds to the direction, where the designer pretends to steer the incident wavefront. Blazed gratings are ubiquitous elements in many applications in optics and photonics, but analogous structures can also be found in other regions of the electromagnetic spectrum as in microwaves-phased antennas.[25,38]

Generally, the diffraction efficiency expressions consider that the gratings are 1D. This is true in LC-OPAs,[24] but when they are addressed onto a 2D SLM, such as the LCoS, we have to consider its 2D pixelated structure. This may affect the theoretical diffraction efficiency calculation, leading to erroneous assessment of the performance of the grating if using the conventional 1D expression. Let us consider, as it is usually the case, that the pixelation has a grid structure, where the pixel period (or pitch) along the two orthogonal directions is the same. We call the spatial coordinates along these directions x_1 and y_1, where we will consider that the modulated profile of the grating is along the x_1 coordinate. Then, the grating addressed onto the 2D pixelation has a separable expression:

$$E(x_1, y_1) = E_x(x_1)E_y(y_1), \tag{1}$$

where $E_x(x_1)$ and $E_y(y_1)$ correspond, respectively, to the profile of the multilevel blazed grating and the pixelation structure in the orthogonal direction. Thus, we focus on the case of beam-steering in one direction, i.e., along a straight line. We note that the extension to steering across a plane can be done by addressing both a blazed profile along x_1 and y_1.[23] Far-field diffraction expression for $E(x_1, y_1)$ results from the product of the far-field expressions for each of the two orthogonal profiles. We note that we recently presented preliminary results for the case of 1D pixelated devices.[39] In the present paper, we extend these results to the case of 2D pixelated devices and discuss the differences arising with respect to the 1D pixelation case.

Let us first derive the expression for light diffracted by the profile described by $E_x(x_1)$ for the multilevel pixelated blazed grating along the x_1 coordinate. We apply a diffraction integral-based[26] calculation since it provides a compact closed expression and combines all the important parameters, as we will show. We partly use the mathematical development presented by Chen et al.,[25] which we complete with the width of the clear aperture of the pixel, necessary to introduce the fill factor parameter, and the possibility of blazed profiles with a phase-depth difference of 2π rad. In a later section, we will further introduce the possibility of the existence of flicker. We will obtain a compact analytical expression enabling to calculate not only the intensity diffracted to the first diffraction order but also to any diffraction order. An expression taking into

account all these factors does not exist in the literature, and we find it useful for further analysis of the experimental measurements and the realistic simulations that will follow in the next sections.

In Fig. 1, we show the image we have taken in our lab of the backplane of one LCoS microdisplay. It corresponds to the commercially available PA-LCoS microdisplay, model PLUTO distributed by the company HOLOEYE. It is a nematic LC filled with 1920×1080 pixels and $0.7''$ diagonal, 8-μm pixel pitch, 93% fill factor, and digitally addressed. This image is similar to other ones found in the literature.[15,32,33] We observe the detail of the structure of interpixel gaps and reflective pixels. Clearly, the interpixel gaps are absorbent, whereas the pixels show high reflectance. We have taken this image with a 20× microscope objective under illumination from a 532-nm diode laser.

In Fig. 1, we show the diagram for the multilevel pixelated blazed profile $E_x(x_1)$ that we want to model with the following parameters: d is the pixel pitch, W is the width of the clear aperture of the pixel, M is the number of levels for the blazed grating, and N is the total number of pixels across the whole grating aperture. We note that the fill factor, a typical specification in pixelated devices, is usually defined in areal terms as $(W/d)^2$.

According to Fig. 2, the electric field for the wavefront after traversing the grating can be considered as composed of two parts:

$$a(x_1) = \sum_{r=0}^{(N/M)-1} \delta(x_1 - rMd), \tag{2a}$$

$$b(x_1) = c_r \sum_{s=0}^{M-1} \exp(js\Delta\phi)\mathrm{rect}\left(\frac{x_1 - sd - W/2}{W}\right), \tag{2b}$$

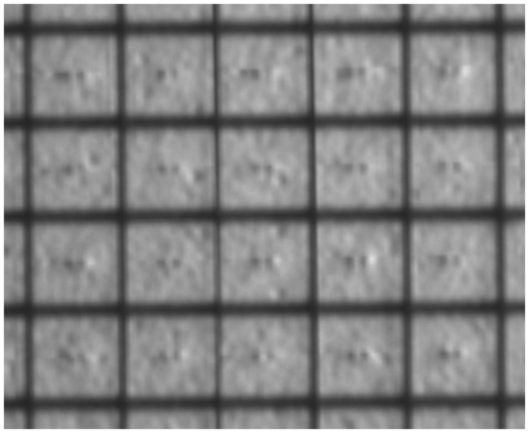

Fig. 1 LCoS backplane: detail of the structure of interpixel gaps and reflective pixels. Pixel pitch is 8 μm.

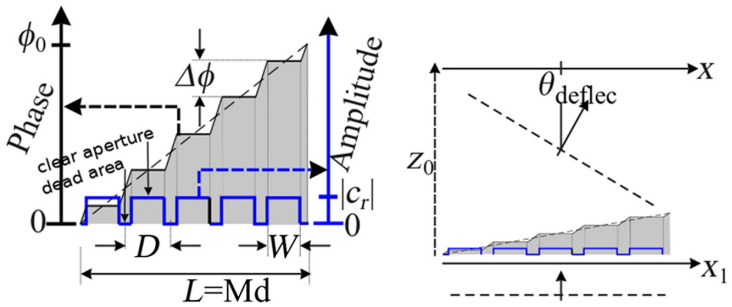

Fig. 2 Diagram of the multilevel blazed grating and the parameters involved.

where $a(x_1)$ describes the periodicity of the blazed profile, $b(x_1)$ is the structure of one period, $\Delta\phi = \phi_0/M$ is the phase step for the M levels composing one period, and ϕ_0 is the phase depth. c_r is a constant factor, which incorporates the losses due to reflection in the interfaces, residual absorption in the different layers of the LCoS structure, and nonunit reflectance of the pixel mirror electrodes. In general, it is a complex number, whose value might depend on the incident wavelength and angle of incidence. Putting everything together we obtain as follows:

$$E_x(x_1) = \left(\sum_{r=0}^{(N/M)-1} \delta(x_1 - rMd)\right) \otimes \left(c_r \sum_{s=0}^{M-1} \exp(js\Delta\phi)\mathrm{rect}\left(\frac{x_1 - sd - W/2}{W}\right)\right), \quad (3)$$

where $\otimes$ is the convolution operation. To obtain the far-field diffraction, we apply the diffraction integral, which in the case of one dimension is given by[26]

$$E_x(x) = \frac{\exp(j\beta z_0)}{j\lambda z_0} \exp\left(j\frac{\beta x^2}{2z_0}\right) \int_{-\infty}^{+\infty} E_x(x_1) \exp\left(-j\frac{\beta}{z_0} x x_1\right) \mathrm{d}x_1, \quad (4)$$

where $E_x(x)$ is the electric field along the x coordinate in the far-field plane at a distance z_0 from the grating plane, λ is the illumination wavelength, and $\beta = 2\pi/\lambda$ is the wavevector. We note that we recently derived some of these expressions.[39] They are partly included in the paper to ease readability. The resultant electric field can be decomposed in three parts as $E_x(x) = c_r E_{x1}(x) E_{x2}(x) E_{x3}(x)$, where $E_{x1}(x)$ is the interaction between periods, $E_{x2}(x)$ is single-slit diffraction, and $E_{x3}(x)$ is multislit interference in one period. To calculate the intensity, we have $I_x(x) = |c_r|^2 A_{x1}(x) A_{x2}(x) A_{x3}(x)$, and if we make the following substitution $u = x/\lambda z_0$, we obtain the expression in terms of spatial frequency u, which is more useful for the purpose of this work. Then, after some algebraic manipulations, we rewrite the three components of the intensity expression as follows:

$$A_{x1}(u) = \left|\frac{\sin(\pi u N d)}{\sin(\pi u M d)}\right|^2, \quad (5a)$$

$$A_{x2}(u) = \left|\frac{\sin(\pi u W)}{\pi u}\right|^2, \quad (5b)$$

$$A_{x3}(u) = \left|\frac{\sin\left(\frac{M}{2}(\Delta\phi - 2\pi u d)\right)}{\sin\left(\frac{1}{2}(\Delta\phi - 2\pi u d)\right)}\right|^2. \quad (5c)$$

We note that the expression $A_{x2}(u)$ contains the effect of the finite extent W of the clear aperture of the pixel. We substitute $\Delta\phi = \phi_0/M$ and combine the three elements together:

$$I_x(u) = |c_r|^2 \left|\frac{\sin(\pi u N d)}{\sin(\pi u M d)}\right|^2 \left|\frac{\sin(\pi u W)}{\pi u}\right|^2 \left|\frac{\sin\left(\frac{1}{2}(\phi_0 - 2\pi u M d)\right)}{\sin\left(\frac{1}{2M}(\phi_0 - 2\pi u M d)\right)}\right|^2. \quad (6)$$

An alternative substitution is also possible, $u = \sin\theta/\lambda \cong \theta/\lambda$ (for small angles), if we want to calculate the angular deflection θ. Usually, in the case of periodic elements, the peak value at the diffraction orders is of interest. Going back to Eq. (6), pixelation orders occur at $u = k_x/d$ and for the periodicity given by the grating period Md, we have that the diffraction orders due to the blazed grating occur at $u = n/Md$. Therefore, pixelation orders coincide with blazed grating orders at $n = k_x M$. Let us obtain the expressions at the blazed grating orders $u = n/Md$. For $A_{x1}(n)$, we apply the l'Hôpital's rule since we get the indeterminate form $0/0$, and we obtain $A_{x1}(n) = |N/M|^2$ independent of n. Then, the intensity value as a function of n is given by

$$I_x(n) = |c_r|^2 \left(\frac{N}{M}\right)^2 \left| \frac{\sin\left(\pi n \frac{W}{Md}\right)}{\pi n \frac{1}{Md}} \right|^2 \left| \frac{\sin\left(\frac{1}{2}(\phi_0 - 2\pi n)\right)}{\sin\left(\frac{1}{2M}(\phi_0 - 2\pi n)\right)} \right|^2. \tag{7}$$

Expressions in Eq. (6) and (7) describe the diffracted intensity in the case of blazed grating profiles displayed onto a 1D pixelated device, i.e., the OPA.

Now, we want to obtain the expression for the case of 2D pixelated devices. Going back to Eq. (1), now, we calculate the far-field diffraction due to the profile $E_y(y_1)$ of pixelation along the orthogonal y_1 coordinate. We consider that the pixel clear aperture, pixel separation, and extent of the grating is the same in both orthogonal directions, so we consider, respectively, the same parameter values d, W, and N as we did along the x_1 coordinate in Eq. (3). Then, the model for the profile of the pixelation can be expressed as follows:

$$E_y(y_1) = \left(\sum_{r=0}^{N-1} \delta(y_1 - rd)\right) \otimes c_r \mathrm{rect}\left(\frac{y_1 - W/2}{W}\right) = c_r \sum_{r=0}^{N-1} \mathrm{rect}\left(\frac{y_1 - rd - W/2}{W}\right). \tag{8}$$

Far-field intensity expression can be obtained from Eqs. (5a)–(5c) by making $M = 1$, then it results as follows:

$$I_y(v) = |c_r|^2 \left| \frac{\sin(\pi v N d)}{\sin(\pi v d)} \right|^2 \left| \frac{\sin(\pi v W)}{\pi v} \right|^2, \tag{9}$$

written as a function of the orthogonal spatial frequency $v = y/\lambda z_0$, where y is the spatial coordinate in the far-field plane along the direction orthogonal to the x coordinate shown in Eq. (4). We rewrite this expression in terms of the pixelation orders, which occur at $v = k_y/d$:

$$I_y(k_y) = |c_r|^2 N^2 \left| \frac{\sin(\pi k_y W/d)}{\pi k_y/d} \right|^2. \tag{10}$$

Then, the expression for the far-field diffraction of the multilevel blazed grating when displayed on a 2D pixelated device is

$$I(u,v) = |c_r|^2 \left| \frac{\sin(\pi u N d)}{\sin(\pi u M d)} \right|^2 \left| \frac{\sin(\pi u W)}{\pi u} \right|^2 \left| \frac{\sin\left(\frac{1}{2}(\phi_0 - 2\pi u M d)\right)}{\sin\left(\frac{1}{2M}(\phi_0 - 2\pi u M d)\right)} \right|^2 \left| \frac{\sin(\pi v N d)}{\sin(\pi v d)} \right|^2 \left| \frac{\sin(\pi v W)}{\pi v} \right|^2, \tag{11}$$

when expressed as a function of the spatial frequency (u, v), and

$$I(n, k_y) = |c_r|^2 N^2 \left(\frac{N}{M}\right)^2 \left| \frac{\sin\left(\pi n \frac{W}{Md}\right)}{\pi n \frac{1}{Md}} \right|^2 \left| \frac{\sin\left(\frac{1}{2}(\phi_0 - 2\pi n)\right)}{\sin\left(\frac{1}{2M}(\phi_0 - 2\pi n)\right)} \right|^2 \left| \frac{\sin(\pi k_y W/d)}{\pi k_y/d} \right|^2, \tag{12}$$

when expressed as a function of the location of the grating orders (n, k_y) in both orthogonal directions.

2.2 *Normalized Efficiency Expressions*

To make the expressions operative, it is necessary to normalize them according to the experimental procedure followed in the measurements. Three different normalizations are possible. We consider unit incident intensity, i.e., unit amplitude of the incident electric field. The first case, normalization 1, considers the total incident power over the illuminated area of the grating. The illuminated area is $(Nd)^2$, which becomes multiplied by the incident unit amplitude and then squared to produce the total incident power is $P_{\mathrm{norm1}} = (Nd)^4$. The second case, normalization 2,

considers the power diffracted to the zero diffraction order when no image is addressed onto the pixelated device. This can be obtained by applying the following substitution in Eq. (12) $(n = 0, k_y = 0)$ and for $\phi_0 = 0$, which results in $P_{\text{norm2}} = |c_r|^2(NW)^4$. The third case, normalization 3, considers the total diffracted power, i.e., the addition of the power at all the diffraction orders. This can be obtained by multiplying the total incident power P_{norm1} by the clear aperture ratio of the pixelated device in areal terms $(W/d)^2$, i.e., the fill factor, and taking into account the constant losses factor $|c_r|^2$, it results in $P_{\text{norm3}} = |c_r|^2N^4(Wd)^2$. This is a heuristic approach, and in the Appendix we have added the mathematical proof for this result.

In Fig. 3, we show how the different normalizations depend with ratio W/d. We have a $(W/d)^2$ dependency for the total transmitted light and $(W/d)^4$ for the light diffracted to the zero pixelation order (no image addressed). For example, this means that for a ratio $W/d = 0.8$, 40% of the incident power is directed to the zero pixelation order, approximately 40% is absorbed in the dead spaces (interpixel gaps) and the remaining 20% is distributed among the rest of diffraction orders. This means that for $W/d = 0.8$, about two-third of the transmitted power goes to the zero order. Then, from the discussion in Fig. 3 and the expressions in Eqs. (11) and (12), the local efficiency $\eta_{\text{DOE,SLM}}(u, v)$ of a programmable DOE with respect to the incident light (normalization 1) can be considered as the product of various components:[40]

$$\eta_{\text{DOE,SLM}}(u, v) = \eta_{\text{trans}}\eta_{0\text{th}}\eta_{\text{sinc}}(u, v)\eta_{\text{DOE}}(u, v), \tag{13}$$

where $\eta_{\text{DOE}}(u, v)$ is the efficiency when the fill factor is 1, η_{trans} is the total transmitted power (normalization 3), and $\eta_{0\text{th}}$ is the fraction diffracted to the zeroth order when no image is addressed. We consider $\eta_{0\text{th}}$ since it is within the zero pixelation order, where the result of the DOE is usually expected. The products η_{trans} and $\eta_{0\text{th}}$ correspond to normalization 2. Then, we have the factor $\eta_{\text{sinc}}(u, v)$, which is equal to $(\text{sinc}(uW)\text{sinc}(vW))^2$, where the sinc is defined as $\text{sinc}(x) \equiv \text{sinc}(\pi x)/(\pi x)$. We note that this $\eta_{\text{sinc}}(u, v)$ is a general factor not only for blazed gratings but for any general DOE as for example diffractive lenses, where it produces the so-called self-apodization[41] or inherent-apodization effect[42] in the impulse response. This decomposition in four terms for $\eta_{\text{DOE,SLM}}(u, v)$ is important since it means that for a general DOE, we can calculate its diffraction efficiency or intensity profile considering a fill factor equal to 1, i.e., which in the case of numerical calculations diminishes the sampling frequency, thus, the computational requirements of memory and time. Afterward, we multiply $\eta_{\text{DOE}}(u, v)$ by the three other factors whose analytical expressions we know.

We show next the explicit expressions when applying the three normalizations to Eq. (12). In particular, we consider the diffracted orders along the direction of deflection by the blazed grating, i.e., $k_y = 0$, since this is the typical case of interest in applications. These are the expressions providing the values of efficiency for each diffracted order of the blazed grating:

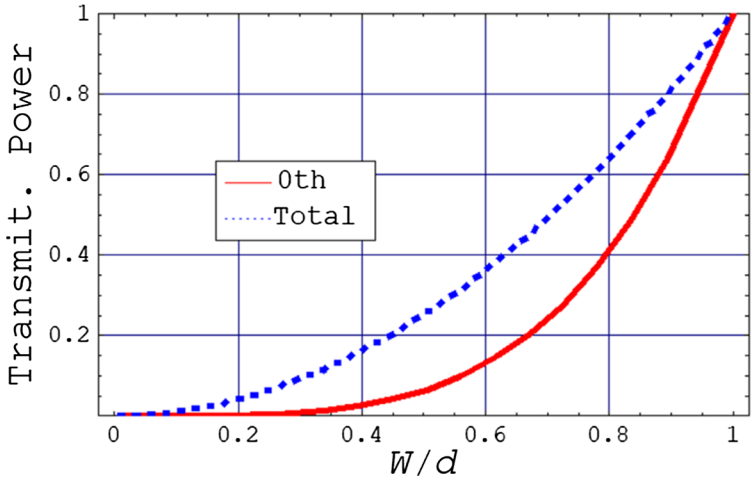

Fig. 3 Limiting effect of the aperture ratio W/d on the transmitted energy for a 2D pixelated device. Dotted curve for the total transmitted light and the continuous curve for the light diffracted onto the zero pixelation order when no image is addressed.

$$\eta_{\text{norm1}}(n, k_y = 0) = |c_r|^2 \left(\frac{1}{Md}\right)^2 \left(\frac{W}{d}\right)^2 \left| \frac{\sin\left(\pi n \frac{W}{Md}\right)}{\pi n \frac{1}{Md}} \right|^2 \left| \frac{\sin\left(\frac{1}{2}(\phi_0 - 2\pi n)\right)}{\sin\left(\frac{1}{2M}(\phi_0 - 2\pi n)\right)} \right|^2, \tag{14a}$$

$$\eta_{\text{norm2}}(n, k_y = 0) = \left(\frac{1}{MW}\right)^2 \left| \frac{\sin\left(\pi n \frac{W}{Md}\right)}{\pi n \frac{1}{Md}} \right|^2 \left| \frac{\sin\left(\frac{1}{2}(\phi_0 - 2\pi n)\right)}{\sin\left(\frac{1}{2M}(\phi_0 - 2\pi n)\right)} \right|^2, \tag{14b}$$

$$\eta_{\text{norm3}}(n, k_y = 0) = \left(\frac{1}{Md}\right)^2 \left| \frac{\sin\left(\pi n \frac{W}{Md}\right)}{\pi n \frac{1}{Md}} \right|^2 \left| \frac{\sin\left(\frac{1}{2}(\phi_0 - 2\pi n)\right)}{\sin\left(\frac{1}{2M}(\phi_0 - 2\pi n)\right)} \right|^2. \tag{14c}$$

When normalized, we see that the values in all Eq. (14) are independent on the extent N of the grating. We note that in experiments, the diffracted intensity is usually normalized by the intensity in the zero order when displaying a uniform screen, i.e., normalization 2. Therefore, Eq. (14b) is the expression theoretically describing most of the experiments in the literature dealing with blazed gratings and other DOEs. We want to remark that we do not find in the literature this complete analytical expression: usually, the fill factor is not considered in the derivation and only the first order or the case for 2π rad phase depth is calculated. These lead to incorrect assessment of experimental values. For example, let us consider the theoretical expression considered in their paper in Eq. (1) by Lingel et al.[15] for the intensity diffracted by a blazed grating written onto a LCoS device. This expression corresponds to the normalization by the total amount of incident light, i.e., normalization 1. Derivation of this expression can be found in the paper by Swanson.[28] It is literally written as follows:

$$\eta_{\text{norm}}(n) = \text{sinc}^2\left(\frac{n}{M}\right) \frac{\text{sinc}^2(n - \phi_0/2\pi)}{\text{sinc}^2[(n - \phi_0/2\pi)/M]}. \tag{15}$$

This can be obtained from our Eq. (14a) when considering the specific case $W = d$. This means that Eq. (15) ignores the fill factor. We note that since the losses factor $|c_r|^2$ is a constant number, it is typically factored out and not taken into account in the expressions in the literature.

It is also important to distinguish the expressions when considering the blazed grating profile displayed onto a 2D pixelated device or onto a linear array, i.e., an OPA. The specific analytical expression when considering a linear array corresponds to Eqs. (6) and (7). In this case, the three normalization powers according to the definitions previously presented are, respectively, $P_{\text{norm1}} = (Nd)^2$, $P_{\text{norm2}} = |c_r|^2(NW)^2$, and $P_{\text{norm3}} = |c_r|^2 N^2(Wd)$. Note that the results are simply obtained from the 2D ones applying the square root since we are now along one dimension. Then, Eq. (7) when normalized results in

$$\eta_{\text{OPA,norm1}}(n) = |c_r|^2 \left(\frac{1}{Md}\right)^2 \left| \frac{\sin\left(\pi n \frac{W}{Md}\right)}{\pi n \frac{1}{Md}} \right|^2 \left| \frac{\sin\left(\frac{1}{2}(\phi_0 - 2\pi n)\right)}{\sin\left(\frac{1}{2M}(\phi_0 - 2\pi n)\right)} \right|^2, \tag{16a}$$

$$\eta_{\text{OPA,norm2}}(n) = \left(\frac{1}{MW}\right)^2 \left| \frac{\sin\left(\pi n \frac{W}{Md}\right)}{\pi n \frac{1}{Md}} \right|^2 \left| \frac{\sin\left(\frac{1}{2}(\phi_0 - 2\pi n)\right)}{\sin\left(\frac{1}{2M}(\phi_0 - 2\pi n)\right)} \right|^2, \tag{16b}$$

$$\eta_{\text{OPA,norm3}}(n) = \left(\frac{1}{M^2 Wd}\right) \left| \frac{\sin\left(\pi n \frac{W}{Md}\right)}{\pi n \frac{1}{Md}} \right|^2 \left| \frac{\sin\left(\frac{1}{2}(\phi_0 - 2\pi n)\right)}{\sin\left(\frac{1}{2M}(\phi_0 - 2\pi n)\right)} \right|^2. \tag{16c}$$

When compared with the expressions for 2D pixelated structure we find that for normalization 1 and 3, the expressions are different. Then, it is important to remember that even though the

blazed grating is along one dimension, the theoretically expected diffraction efficiency to be used varies if the pixelation structure of the device where it is displayed is 1D or 2D. Only in the case of normalization 2, or in the micro-optics DOEs case for which $W = d$, expressions for OPA or for 2D structure are the same.

2.3 *Application to Blazed Gratings with Flicker*

Once we have the analytical expressions for the far-field diffraction for the blazed grating, they can be used to produce more specific expressions for different situations. One such situation is when the pixelated device exhibits temporal fluctuations, also called flicker, in the phase value addressed, as it is the case in most of LCoS devices.[9–11] Let us now model the existence of flicker. To this goal, we consider that the phase depth fluctuates in time $\phi_0(t)$ with a triangular profile,[9,11] where $\bar{\phi}_0$ is the average phase depth and $2a$ is the peak-to-peak fluctuation:

$$\phi_0(t) = \begin{cases} \bar{\phi}_0 - a + \frac{2a}{T/2}t & 0 \le t < T/2 \\ \bar{\phi}_0 + 3a - \frac{2a}{T/2}t & T/2 \le t < T \end{cases}. \tag{17}$$

Then, we do the averaged calculation for the numerator and the denominator in the phase depth-dependent term in the equations in the previous section. From the averaging, we obtain as follows:

$$\left\langle \sin\left(\frac{1}{2}(\phi_0(t) - 2\pi n)\right)\right\rangle = \frac{\sin(a/2)}{a/2}\ \sin\left(\frac{\bar{\phi}_0 - 2\pi n}{2}\right), \tag{18a}$$

$$\left\langle \sin\left(\frac{1}{2M}(\phi_0(t) - 2\pi n)\right)\right\rangle = \frac{\sin(a/(2M))}{a/(2M)}\ \sin\left(\frac{\bar{\phi}_0 - 2\pi n}{2M}\right). \tag{18b}$$

In Eqs. (14) and (16), we have to apply this substitution to the phase-dependent term to produce the averaged expression in the presence of flicker. For example, in the case of Eq. (14b), we obtain:

$$\bar{I}_{\text{norm2}}(n, k_y = 0) = \left(\frac{1}{MW}\right)^2 \left|\frac{\sin\left(\pi n \frac{W}{Md}\right)}{\pi n \frac{1}{Md}}\right|^2 \left|\frac{\frac{\sin(a/2)}{a/2}\ \sin\left(\frac{1}{2}(\bar{\phi}_0 - 2\pi n)\right)}{\frac{\sin(a/(2M))}{a/(2M)}\ \sin\left(\frac{1}{2M}(\bar{\phi}_0 - 2\pi n)\right)}\right|^2. \tag{19}$$

3 Simulated Results and Discussion

3.1 *Far-Field Profile*

We have obtained both the expressions for the diffraction efficiency at the different orders and also the expressions for the far-field intensity profile. In the following, through simulations, we will show the interest and potential of our analytical approach. We will consider the typical case of interest in most applications, when the diffracted orders are along the direction of deflection by the blazed grating, i.e., $k_y = 0$ in the 2D expressions.

First, we focus on the intensity profile, which enables to calculate the location and width of the different maxima and their sidelobes. One possible application, for example, is to calculate the cross talk due to higher orders in multichannel interconnects.[19] We want to show the kind of information that can be extracted from each of the three normalizations. We also want to show what is the effect of the fill factor on the diffracted intensity profile. In the simulations, we will consider the three following cases: $W = d$, $W = 0.9d$, and $W = 0.7d$. The first case $W = d$ is what is usually considered in many papers in spite of the fact that SLMs have a fill factor smaller than one. Then, most of LCoS nowadays have values between $W = d$ and $W = 0.9d$, as can be seen in Table 1 in the paper by Zhang et al.[6]. And the case $W = 0.7d$ is in the range exhibited by transmissive liquid crystal displays,[42] which were the dominant technology before LCoS

microdisplays. Without any loss of generality, we note that in the following, we consider the constant losses factor $|c_r|^2$ is equal to 1.

In Figs. 4(a1)–4(c1), first row, we show, respectively, for $W = d$, $W = 0.9d$, and $W = 0.7d$, the intensity profile applying normalization 1 as a function of the spatial frequency in units of the pixelation orders. We note that an alternative plot can be obtained substituting $u = \sin\theta/\lambda$ to calculate the angular deflection θ. We are interested in showing how the blazed grating orders expand along the pixelation orders. In normalization 1, the intensity values were given by Eq. (11) for the 2D pixelated device are divided by the total amount of incident light $(Nd)^4$. The three curves in each of the plots correspond to the simulated results for the number M of quantization levels 2, 5, and 12, given in the legend, and for a phase depth of 2π rad. We further add the curve for the sinc function $(W^2\,\mathrm{sinc}(uW))^2$, resulting from the term in Eq. (5b), which contains the effect of the finite extent W of the clear aperture of the pixel. We note that the sinc behaves as an envelope limiting the maximum intensity for the diffracted orders by each of the gratings. When the fill factor decreases, from the first to the third column, the sinc lowers its height since a larger part of the incident light is being absorbed in the dead spaces (interpixel gaps). We see that there are blazed grating diffracted orders across the whole output plane. Actually, we might think that at each of the pixelation orders, the diffracted orders by the blazed grating are replicated. We see that at the zero pixelation order, the first order for each of the three gratings (given in the legend) is to the right. Then, at each of the pixelation orders, we see that this repeats but with a different intensity height due to the limiting sinc function. The larger the number of levels, the larger the intensity of the first diffracted order in the zero pixelation order and the closer to the center.

In Figs. 4(a2)–4(c2), second row, we show the results when applying normalization 2, where the intensity values in Eq. (11) are divided by power transmitted to the zero diffracted order when no image is addressed onto the pixelated device, which is $(NW)^4$. This is the normalization usually applied when taking experimental measurements in the lab. Now, the sinc curve represented is $(\mathrm{sinc}(uW))^2$, which works as the envelope for the intensity at the different diffracted orders by the blazed grating. Since the sinc curves are now normalized to one, it is more visible how the width of the central maxima and sidelobes increases as the clear aperture W decreases.

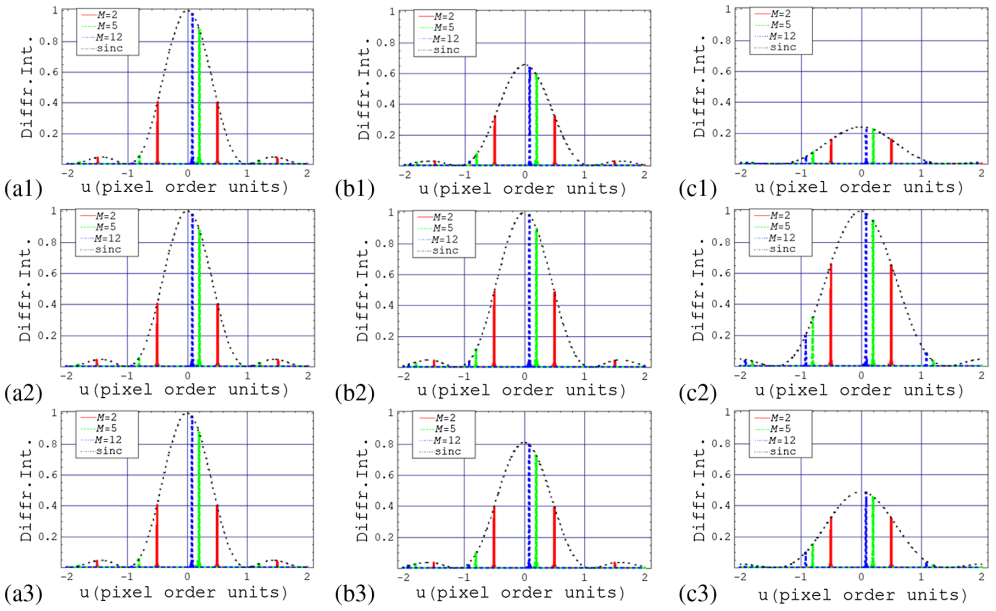

Fig. 4 Intensity profile for the blazed grating far-field as a function of the spatial frequency (in terms of the pixelation orders). We consider a phase-depth of 2π. In the legend, the three values for the number M of quantization levels. We consider the three normalizations for a 2D pixelated device: normalization 1, 2, and 3, respectively, for the first (a1–c1), second (a2–c2), and third (a3–c3) rows. We consider three different pixel apertures: $W = d$, $W = 0.9d$, and $W = 0.7d$ for the first (a1–a3), second (b1–b3), and third (c1–c3) columns.

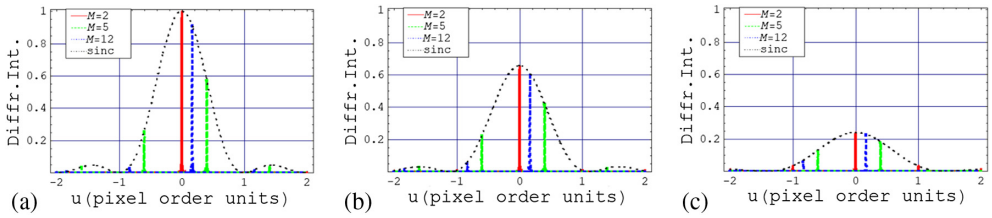

Fig. 5 Intensity profile for the blazed grating far-field as a function of the spatial frequency (in terms of the pixelation orders). We consider a phase depth of 4π and normalization 1 for a 2D pixelated device. In the legend, the three values for the number M of quantization levels: (a) $W = d$, (b) $W = 0.9d$, and (c) $W = 0.7d$.

The plots in this second row can be obtained from the ones in the first row by multiplying $(W/d)^4$.

For the sake of completeness, we show in Figs. 4(a3)–4(c3), third row, the equivalent results when applying normalization 3: intensity values in Eq. (11) are divided by the total transmitted power, which is $N^4(Wd)^2$. In this case, the sinc curve working as an envelope for the diffracted intensity is represented by $(W\,\mathrm{sinc}(uW))^2$. This plot can then be obtained by multiplying the plots in the second row by $(W/d)^2$. We note that results for $W = d$ (first column) are the same for the three rows [Figs. 4(a1)–4(a3)].

A notable capability of the expressions derived is that they are not limited to the case of 2π rad phase depth. There is an interest in multiorder DOEs,[43–45] where the capability of some LCoS devices to possess a modulation range multiple of 2π rad is exploited. In Fig. 5, we show the intensity profile (normalization 1) for the blazed grating for a 4π rad phase depth. The same ratios, W/d, and number of quantization levels are considered as in Fig. 4. When compared with the first row in Fig. 4, we see that the blazed grating diffraction orders at all the pixelation orders have moved to the right double the distance. Then, deflection is twice and efficiency is smaller due to the limiting sinc envelope. A limiting case results for $M = 2$, where we see that light is directed to the zero pixelation order. This can be understood that double the distance means that the blazed grating order originally within the minus first pixelation order in Fig. 4, at $u = -0.5$, is now shifted to $u = 0$. Correspondingly, the one at $u = 0.5$ in Fig. 4 is now at $u = 1$. An important result we obtain is that, because of the limiting sinc envelope produced by the pixel aperture, the location and efficiency of the order n for a blazed grating with a period M and phase depth 2π rad is identical to the location and efficiency of the order kn for a grating with a period kM and phase depth k2π rad, where k is an integer.

We note that the results we obtain do not take into account the existence of interpixel cross talk effects, such as the fringing-field.[14,15,33,46] Our model is not considering this degradation effect. The results we produce show the ideal limiting case, which is the situation approached when the pixel period of the grating increases or when the ratio of the cell gap to the pixel pitch is small.[14,15,33,46] When the pixel period decreases, fringing field increases and the diffraction efficiency values reduce. In this situation, Sun et al.[46] have shown that 4π rad multiorder blazed gratings might produce larger diffraction efficiency values when compared with their equivalent 2π rad generating the same deflection angle. However, the diffraction efficiency values are in any case lower than the ideal limiting values.

3.2 *Diffraction Efficiency*

The expressions obtained enable to calculate the diffraction efficiency at the different orders, which is the usual concern for diffraction gratings, where this efficiency is typically maximized at the first order $n = 1$. In the following, we show how the diffraction efficiency values at the first order are affected by the set of parameters introduced in this work. Let us consider, without any loss of generality, that the constant losses factor $|c_r|^2$ is equal to 1.

In Figs. 6(a1)–6(c1), respectively, for the normalizations 1, 2, and 3, we show the diffraction efficiency versus the number of quantization levels for blazed grating onto 2D pixelated devices. We consider the three pixel apertures W (in the legend) considered in Figs. 4 and 5 previously.

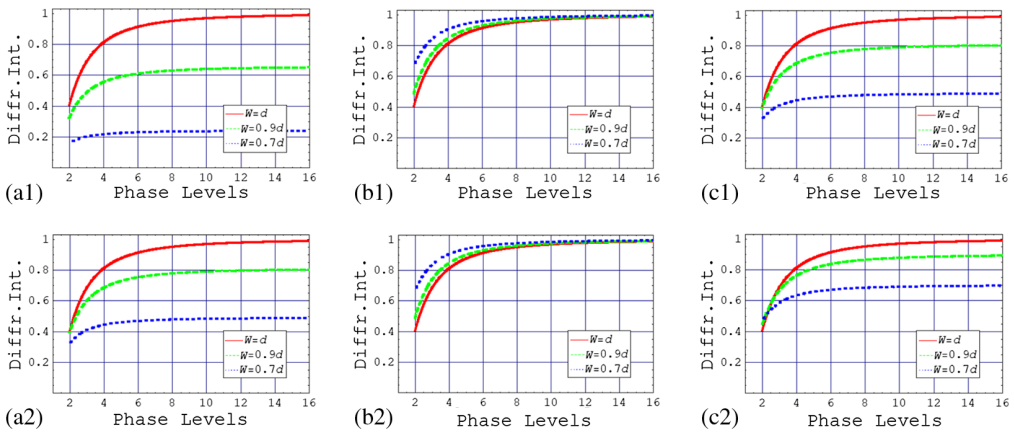

Fig. 6 Intensity diffracted to the first grating order $n = 1$ as a function of the number of quantization levels of the blazed grating: phase depth of 2π rad and no flicker. In the legend, the three values for the pixel aperture W. (a1–c1) and (a2–c2) We show the cases for 2D and 1D pixelated devices, respectively, in the first and second rows, and for the three normalizations: normalization 1, 2, and 3, respectively, in the first (a1, a2), second (b1, b2), and third columns (c1, c2).

The phase-depth applied is 2π rad and there is no flicker. The continuous line corresponds to the case $W = d$, whose values are usually considered as the reference of the maximum reachable diffraction efficiency. For example, for $M = 2$, efficiency is 40.5%, which increases rapidly with the number of levels to such high values as 95.0% for $M = 8$. We see that when $W \neq d$, the diffraction efficiency does not coincide with the continuous curve. Actually, depending on the normalization, the efficiencies are lower (normalization 1 and 3) but they can also be higher (normalization 2). We see in the case of normalization 2, the usual one applied in experiments that the values can be significantly higher with respect to the case $W = d$, especially for low number of levels: for $M = 2$, the efficiency is 48.8% and 65.7%, respectively, for $W = 0.9d$ and $W = 0.7d$; and for $M = 8$, the values are 95.9% and 97.5%, respectively, for $W = 0.9d$ and $W = 0.7d$. In Figs. 6(a2)–6(c2), second row, we show the results equivalent to the ones in Figs. 6(a1)–6(c1) but now for 1D pixelated devices. We see that the curve for $W = d$ is identical between the 2D and 1D pixelated devices. Then, for normalization 2, Figs. 6(b1) and 6(b2) are also identical.

We have demonstrated the differences produced because of the fill factor and the 1D and 2D pixelated geometries. Next, we want to show the influence of the pixel aperture combined with the flicker on the calculated diffraction efficiency at the first grating order $n = 1$. In Fig. 7, for normalization 2 (Eq. (19)), we show these simulations as a function of the number of phase levels, for no flicker (a), with flicker $a = 20$ deg (b), and with flicker $a = 40$ deg (c). In each of the plots, we display the curves for the three pixel apertures (in the legend). As we have already commented in Fig. 6, the diffraction efficiency depends on the fill factor. If we focus on the effects of flicker, as we go from the plot (a) to plot (c), flicker increases and, as a result, we see that the diffraction efficiency decreases. Change is very small between Figs. 7(a) and 7(b), and becomes more visible between Figs. 7(b) and 7(c), especially for larger number of quantization levels. However, we note that even for such a large flicker amplitude of $a = 40$ deg, the decrease in diffraction efficiency at a large number of quantization levels is only about 5%. This is consistent with the results in our previous paper,[18] where we concluded that the effect of flicker in programmable DOEs is not that important and it is very much application dependent. In contrast, in interferometry,[10] it is absolutely necessary to have minimal values of flicker.

4 Conclusions

Applying the diffraction integral, we have obtained the diffracted field for blazed gratings displayed onto pixelated devices. These analytical expressions take into account the fill factor and the existence of flicker, which are characteristics of SLMs and in particular of LCoS

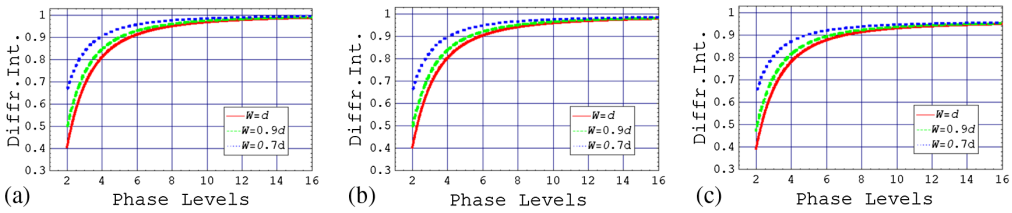

Fig. 7 Intensity diffracted to the first grating order $n = 1$ as a function of the number of quantization levels of the blazed grating, for a phase depth of 2π rad, applying normalization 2 for 2D pixelated devices. In the legend, the three values for the pixel aperture W considered. (a) No flicker, (b) flicker, $a = 20$ deg, and (c) flicker, $a = 40$ deg.

microdisplays. The analytical expression also includes the phase depth and the number of quantization levels; thus, it is a very comprehensive equation not existent, to the best of our knowledge, in the literature. Three different experimental-based normalizations are considered. This is important since we have found that they may lead to wrong conclusions if the fill factor is not considered in the expressions. Furthermore, in most of the literature dealing with LCoS devices, the conventional expressions used are the ones that were derived for micro-optics DOEs, where no fill factor parameter is needed, thus leading to wrong results when applied to programmable DOEs. We have compared the diffracted field expressions for 1D and 2D pixelated devices, and we have found that there are differences between them when fill factor is smaller than 1. When compared with numerical procedures, our approach provides a comprehensive analytical expression, which facilitates the design, prediction, and discussion of experiments. As an application, we prove that multiorder DOEs cannot be more efficient than the equivalent single-order DOE, valid at least for the limiting case of no interpixel cross talk. We also show how the results for DOEs with a unit fill factor can be adapted to DOEs with a fill factor smaller than 1 with a very efficient procedure. We have also simulated the impact of flicker on the diffraction efficiency: flicker must be very high to impact significantly on the diffraction efficiency.

5 Appendix: Total Transmitted Power by a Pixelated Device

Let us consider, without any loss of generality, that the constant losses factor $|c_r|^2$ is equal to 1. Applying Eq. (10) along with both coordinates, we obtain the expression:

$$I(k_x, k_y) = N^4 \left| \frac{\sin(\pi k_x W/d)}{\pi k_x/d} \right|^2 \left| \frac{\sin(\pi k_y W/d)}{\pi k_y/d} \right|^2, \tag{20}$$

which provides the diffracted intensity for the pixelation orders produced by a 2D pixelated device. If we are able to add these intensities for all of the infinite orders, then we will have found the total transmitted light by the pixelated device, i.e., normalization 3. We start with the summation:

$$\text{Norm3} = N^4 \sum_{k_x=-\infty}^{+\infty} \left| \frac{\sin(\pi k_x W/d)}{\pi k_x/d} \right|^2 \sum_{k_y=-\infty}^{+\infty} \left| \frac{\sin(\pi k_y W/d)}{\pi k_y/d} \right|^2. \tag{21}$$

From the heuristic approach in Sec. 2.2, $\text{Norm3} = N^4 (Wd)^2$. Then, we must prove that

$$\sum_{k=-\infty}^{+\infty} \left| \frac{\sin(\pi k x)}{\pi k} \right|^2 = x, \tag{22}$$

where $x = W/d$. Taking into account that the term $k = 0$ in the summation is equal to x^2 (applying l'Hôpital's rule), then the summation can be expressed as follows:

$$\sum_{k=-\infty}^{+\infty}\left|\frac{\sin(\pi kx)}{\pi k}\right|^2 = x^2 + 2\sum_{k=1}^{+\infty}\left|\frac{\sin(\pi kx)}{\pi k}\right|^2, \tag{23}$$

and Eq. (22) becomes

$$2\sum_{k=1}^{+\infty}\left|\frac{\sin(\pi kx)}{\pi k}\right|^2 = x - x^2. \tag{24}$$

We use the identity $\sin^2(x) = (1-\cos(2x))/2$:

$$\sum_{k=1}^{+\infty}\frac{1-\cos(2\pi kx)}{(\pi k)^2} = x - x^2. \tag{25}$$

And

$$\sum_{k=1}^{+\infty}\frac{1}{(\pi k)^2} - \sum_{k=1}^{+\infty}\frac{\cos(2\pi kx)}{(\pi k)^2} = x - x^2. \tag{26}$$

Then, we calculate the Fourier series expansion for the two terms on the right side:

$$x = \frac{1}{2} + \sum_{k=1}^{+\infty}\frac{-1}{\pi k}\sin(2\pi kx), \tag{27a}$$

$$x^2 = \frac{1}{3} + \sum_{k=1}^{+\infty}\left[\frac{1}{(\pi k)^2}\cos(2\pi kx) + \frac{-1}{\pi k}\sin(2\pi kx)\right], \tag{27b}$$

which produce

$$x - x^2 = \frac{1}{6} - \sum_{k=1}^{+\infty}\frac{\cos(2\pi kx)}{(\pi k)^2}. \tag{28}$$

And taking into account the series $\sum_{k=1}^{+\infty} 1/k^2 = \pi^2/6$, then both sides in Eq. (26) are identical and the proof for Eq. (22) has been completed.

Acknowledgments

This work was funded by Ministerio de Economía, Industria y Competitividad (Spain), projects FIS2017-82919-R (MINECO/AEI/FEDER, UE) and FIS2015-66570-P (MINECO/FEDER); by Generalitat Valenciana (Spain), project PROMETEO II/2015/015 and GV/2019/021; and Universidad de Alicante (Spain), project GRE17-06.

References

1. N. Savage, "Digital spatial light modulators," *Nat. Photonics* **3**, 179–179 (2009).
2. C. Rosales-Guzmán and A. Forbes, *How to Shape Light with Spatial Light Modulators*, SPIE Press, Bellingham, Washington (2017).
3. A. Márquez et al., "Programmable apodizer to compensate chromatic aberration effects using a liquid crystal spatial light modulator," *Opt. Express* **13**, 716–730 (2005).
4. A. Farré et al., "Positional stability of holographic optical traps," *Opt. Express* **19**, 21370–21384 (2011).
5. M. A. F. Roelens et al., "Dispersion trimming in a reconfigurable wavelength selective switch," *J. Lightwave Technol.* **26**, 73–78 (2008).
6. Z. Zhang, Z. You, and D. Chu, "Fundamentals of phase-only liquid crystal on silicon (LCoS) devices," *Light Sci. Appl.* **3**, 1–10 (2014).

7. G. Lazarev et al., "Beyond the display: phase-only liquid crystal on Silicon devices and their applications in photonics," *Opt. Express* **27**, 16206–16249 (2019).
8. A. Márquez and A. Lizana, "Special issue on liquid crystal on silicon devices: modeling and advanced spatial light modulation applications," *Appl. Sci.* **9**, 3049 (2019).
9. A. Lizana et al., "Time fluctuations of the phase modulation in a liquid crystal on silicon display: characterization and effects in diffractive optics," *Opt. Express* **16**, 16711–16722 (2008).
10. J. García-Márquez et al., "Flicker minimization in an LCoS spatial light modulator," *Opt. Express* **20**, 8431–8441 (2012).
11. F. J. Martínez et al., "Averaged Stokes polarimetry applied to evaluate retardance and flicker in PA-LCoS devices," *Opt. Express* **22**, 15064–15074 (2014).
12. F. J. Martínez et al., "Electrical dependencies of optical modulation capabilities in digitally addressed parallel aligned LCoS devices," *Opt. Eng.* **53**, 067104 (2014).
13. H. Yang and D. P. Chu, "Phase flicker optimisation in digital liquid crystal on silicon devices," *Opt. Express* **27**, 24556–24567 (2019).
14. B. Apter, U. Efron, and E. Bahat-Treidel, "On the fringing-field effect in liquid-crystal beam-steering devices," *Appl. Opt.* **43**, 11–19 (2004).
15. C. Lingel, T. Haist, and W. Osten, "Optimizing the diffraction efficiency of SLM-based holography with respect to the fringing field effect," *Appl. Opt.* **52**, 6877–6883 (2013).
16. F. J. Martínez et al., "Effective angular and wavelength modelling of parallel aligned liquid crystal devices," *Opt. Lasers Eng.* **74**, 114–121 (2015).
17. J. Francés et al., "Simplified physical modeling of parallel-aligned liquid crystal devices at highly non-linear tilt angle profiles," *Opt. Express* **26**, 12723–12741 (2018).
18. F. J. Martínez et al., "Predictive capability of average Stokes polarimetry for simulation of phase multilevel elements onto LCoS devices," *Appl. Opt.* **54**, 1379–1386 (2015).
19. D. Gil-Leyva et al., "Cross-talk analysis in a telecentric adaptive free-space optical relay based on a spatial light modulator," *Appl. Opt.* **45**, 63–75 (2006).
20. M. Salsi et al., "Mode-division multiplexing of 2 100 Gb/s channels using an LCOS-based spatial modulator," *J. Lightwave Technol.* **30**, 618–623 (2012).
21. M. Wang et al., "LCoS SLM study and its application in wavelength selective switch," *Photonics* **4**(22), 1–16 (2017).
22. L. Wu et al., "Steering performance of oblique arriving beam backward propagating through one-dimensional liquid crystal optical phased array," *Opt. Eng.* **55**(11), 116115 (2016).
23. F. Feng, I. H. White, and T. D. Wilkinson, "Free space communications with beam steering a two-electrode tapered laser diode using liquid-crystal SLM," *J. Lightwave Technol.* **31**, 2001–2007 (2013).
24. P. F. McManamon et al., "Optical phased array technology," *Proc. IEEE* **84**(2), 268–298 (1996).
25. J. Chen et al., "Grating lobes analysis based on blazed grating theory for liquid crystal optical-phased array," *Opt. Eng.* **52**(9), 97102 (2013).
26. J. W. Goodmann, *Introduction to Fourier-Optics*, 3rd ed., Roberts & Company, Greenwood Village, Colorado (2005).
27. I. Moreno et al., "Effects of amplitude and phase mismatching errors in the generation of a kinoform for pattern recognition," *Jpn. J. Appl. Phys.* **34**, 6423–6432 (1995).
28. G. J. Swanson, "Binary optics technology: theoretical limits on the diffraction efficiency of multilevel diffractive optical elements," MIT Technical Report 914, MIT, Cambridge, Massachusetts (1991).
29. H. P. Herzig, Ed., *Micro-Optics: Elements, Systems and Applications*, 1st ed., Taylor and Francis, London (1997).
30. J. Turunen and F. Wyrowski, Eds., *Diffractive Optics for Industrial and Commercial Applications*, Akademie Verlag, Berlin (1997).
31. S. T. Wu and D. K. Yang, *Reflective Liquid Crystal Displays*, John Wiley & Sons Inc., Somerset, New Jersey (2005).
32. T. Lu et al., "Pixel-level fringing-effect model to describe the phase profile and diffraction efficiency of a liquid crystal on silicon device," *Appl. Opt.* **54**, 5903–5910 (2015).

33. K. H. F. Chian and S. T. Wu, "Fringing-field effects on high-resolution liquid crystal microdisplays," *J. Disp. Technol.* **1**(2), 304–313 (2005).
34. D. Armitage, I. Underwood, and S. T. Wu, *Introduction to Microdisplays*, John Wiley & Sons Inc., Hoboken, New Jersey (2006).
35. I. Underwood, "Liquid crystal on silicon reflective microdisplays," in *Handbook of Visual Display Technology*, J. Chen, W. Cranton, and M. Fihn, Eds., Springer, Cham (2016).
36. H. Yang and D. P. Chu, "Digital phase-only liquid crystal on silicon device with enhanced optical efficiency," *OSA Continuum* **2**, 2445–2459 (2019).
37. S. Moser, M. Ritsch-Marte, and G. Thalhammer, "Model-based compensation of pixel crosstalk in liquid crystal spatial light modulators," *Opt. Express* **27**, 25046–25063 (2019).
38. S. Yin et al., "Ultra-fast speed, low grating lobe optical beam steering using unequally spaced phased array technique," *Opt. Commun.* **270**(1), 41–46 (2007).
39. A. Márquez et al., "Blazed grating theory to minimize the non-idealities in LCoS devices," *Proc. SPIE* **11136**, 1113613 (2019).
40. I. Moreno et al., "Modulation light efficiency of diffractive lenses displayed onto a restricted phase-mostly modulation display," *Appl. Opt.* **43**, 6278–6284 (2004).
41. V. Arrizón, E. Carreón, and L. A. González, "Self apodization of low-resolution pixelated lenses," *Appl. Opt.* **38**, 5073–5077 (1999).
42. M. J. Yzuel et al., "Inherent apodization of lenses encoded on liquid-crystal spatial light modulators," *Appl. Opt.* **39**, 6034–6039 (2000).
43. J. Albero et al., "Second order diffractive optical elements in a spatial light modulator with large phase dynamic range," *Opt. Lasers Eng.* **51**, 111–115 (2013).
44. V. Calero et al., "Liquid crystal spatial light modulator with very large phase modulation operating in high harmonic orders," *Opt. Lett.* **38**, 4663–4666 (2013).
45. E. Pérez-Cabré and M. S. Millán, "Liquid crystal spatial light modulator with optimized phase modulation ranges to display multiorder diffractive elements," *Appl. Sci.* **9**, 2592 (2019).
46. C. Sun et al., "High-efficiency beam steering LCOS for wavelength selective switch," *IEEE Photonics Technol. Lett.* **30**(19), 1683–1686 (2018).

Andrés Márquez received his MSc (1997) and PhD (2001) degrees in physics from the Universidad Autónoma de Barcelona. Since 2000, he is with the Group of Holography and Optical Processing, Universidad de Alicante, where he is the professor of applied physics. His focus is in holographic recording materials, liquid crystal spatial light modulators, optical image processing, and diffractive optics with more than 100 articles in journals in the JCR and more than 70 in *Proceedings of SPIE*.

Francisco J. Martínez-Guardiola was graduated in electronic engineering in 1996 and in physics in 1999 from the University of Valencia. He received his PhD from the University of Alicante in 2015. His research is focused on holography and holographic data storage systems. He has authored more than 10 scientific publications on the mentioned subjects in JCR indexed journals and more than 10 in *Proceedings of SPIE*. He is an assistant professor at the University of Alicante.

Jorge Francés received his PhD at the University of Alicante in 2011. He received his MSEE in 2009 and his BSEE in 2006, both from the Technical University of Valencia, Valencia, Spain. Since 2008, he is with the Group of Holography and Optical Processing, Universidad de Alicante, where he also works as a lecturer. His main research interests include physical optics, sound and vibration, and numerical simulation.

Cristian Neipp received his MSc (1996) and PhD (2001) degrees in physics, respectively, from the University of Salamanca and the University of Alicante. He has taught applied physics for engineering students since 1998. Since 1998, he is with the Group of Holography and Optical Processing, Universidad de Alicante, where he is a professor of applied physics. He is mainly interested in holography, holographic recording materials, holographic optical elements, optical processing, electromagnetic theory of diffraction and volume gratings, and physics and

engineering education. In these areas, he has published more than 130 technical papers in various journals and presented more than 100 papers in scientific conferences and congresses.

Manuel G. Ramírez obtained his BSc (2007) degree in chemistry from the University of Valencia. He received his MsC (2010) and PhD (2013) degrees from the University of Alicante. He has worked in organic solid-state lasers, mesoporous materials doped with organic active molecules, preparation and modification of carbon nanoforms by mechanochemical methods, functionalization and optoelectronics properties of graphene quantum dots, and development of the solid-state laser based on conjugated polymers. Currently, he carries out his research in the field of holography and photopolymer materials in the holography and optical processing in the University of Alicante. He has published 17 articles in journals in the JRC.

Eva M. Calzado was graduated in physics in 2000 from the University of Valencia, Spain, and received her PhD (with honors) from the University of Alicante, Spain, in 2008. Her research is focused on organic electronics, development of organic solid-state distributed feedback (DFB) laser, and material for laser applications identifying the presence of amplified spontaneous emission (ASE).

Marta Morales-Vidal received her MSc (2012) and PhD (2015) degrees in nanoscience and molecular nanotechnology from the University of Alicante (UA). Since January 2019, she is with the Group of Holography and Optical Processing and the UA Institute of Physics Applied to Science and Technology, where she directs a research project. Her focus is related to laser technologies, advanced optical materials, and biosensing, with more than 10 JCR-Q1 articles in the last 7 years.

Sergi Gallego was graduated in physics in 2001 from the University of Valencia, Spain, and received his PhD (with honors) from the University of Alicante, Spain, in 2005. His research is focused on holography, holographic recording materials, LCDs for holographic applications, electromagnetic theory, holographic and diffractive optical elements, and holographic data storage. He coauthored one patent and more than 80 scientific publications on the above-mentioned subjects in journals indexed in Journal Citation Reports (ISI).

Augusto Beléndez received his MSc and PhD degrees in physics from the University of Valencia in 1986 and 1990, respectively. In 1996, he became a full professor of applied physics at the University of Alicante. He is mainly interested in holography, holographic recording materials, holographic optical elements, liquid crystal spatial light modulators, and diffractive optics. This research has generated more than 230 publications in journals indexed in the JCR and 75 in *Proceedings of SPIE*.

Inmaculada Pascual received her MSc (1985) and PhD (1990) degrees in physics from the University of Granada and University of Valencia, respectively. In 1986, she joined the University of Alicante, where she was appointed as a full professor of optics in 2000. She has carried out research in holographic recording material, holographic memories, and optical elements in green photonics. This research has generated more than 125 publications in journals indexed in the JCR and 52 in *Proceedings of SPIE*.